Cell Reports
Article

TDP-43 Loss-of-Function Causes Neuronal Loss Due to Defective Steroid Receptor-Mediated Gene Program Switching in *Drosophila*

Lies Vanden Broeck,[1,3,4] Marina Naval-Sánchez,[2] Yoshitsugu Adachi,[5] Danielle Diaper,[5] Pierre Dourlen,[4] Julien Chapuis,[4] Gernot Kleinberger,[6,7] Marc Gistelinck,[1,3,4] Christine Van Broeckhoven,[6,7] Jean-Charles Lambert,[4] Frank Hirth,[5] Stein Aerts,[2] Patrick Callaerts,[1,3,*] and Bart Dermaut[1,3,4,*]

[1]Laboratory of Behavioral and Developmental Genetics
[2]Laboratory of Computational Biology
Center of Human Genetics, University of Leuven, B3000 Leuven, Belgium
[3]VIB Center for the Biology of Disease, B3000 Leuven, Belgium
[4]INSERM U744, Institut Pasteur de Lille, Université de Lille Nord de France, 59019 Lille, France
[5]Department of Neuroscience, Institute of Psychiatry, MRC Centre for Neurodegeneration Research, King's College London, SE5 8AF London, UK
[6]Department of Molecular Genetics, Neurodegenerative Brain Diseases Group, VIB, B2610 Antwerpen, Belgium
[7]Laboratory of Neurogenetics, Institute Born-Bunge, University of Antwerp, B2610 Antwerpen, Belgium
*Correspondence: patrick.callaerts@cme.vib-kuleuven.be (P.C.), bart.dermaut@pasteur-lille.fr (B.D.)
http://dx.doi.org/10.1016/j.celrep.2012.12.014

SUMMARY

TDP-43 proteinopathy is strongly implicated in the pathogenesis of amyotrophic lateral sclerosis and related neurodegenerative disorders. Whether TDP-43 neurotoxicity is caused by a novel toxic gain-of-function mechanism of the aggregates or by a loss of its normal function is unknown. We increased and decreased expression of *TDP-43* (*dTDP-43*) in *Drosophila*. Although upregulation of *dTDP-43* induced neuronal ubiquitin and dTDP-43-positive inclusions, both up- and downregulated *dTDP-43* resulted in selective apoptosis of bursicon neurons and highly similar transcriptome alterations at the pupal-adult transition. Gene network analysis and genetic validation showed that both up- and downregulated *dTDP-43* directly and dramatically increased the expression of the neuronal microtubule-associated protein Map205, resulting in cytoplasmic accumulations of the ecdysteroid receptor (EcR) and a failure to switch EcR-dependent gene programs from a pupal to adult pattern. We propose that dTDP-43 neurotoxicity is caused by a loss of its normal function.

INTRODUCTION

TDP-43 plays a crucial role in amyotrophic lateral sclerosis (ALS) and related TDP-43 proteinopathies, such as frontotemporal dementia (FTD) (Sreedharan et al., 2008; Arai et al., 2006; Neumann et al., 2006; Kabashi et al., 2008). In these disorders TDP-43-positive inclusions are often located in the neuronal cytoplasm and accompanied by a loss of nuclear TDP-43 expression. As a result both cytoplasmic toxic gain-of-function (GOF) and nuclear loss-of-function (LOF) mechanisms have been proposed (Lee et al., 2011; Xu, 2012). TDP-43 functions in RNA metabolism, including splicing, transcription, and RNA stability (Budini et al., 2011). Recent studies showed that expression levels and alternative splicing of a large number of neuronal transcripts, including noncoding RNAs, are regulated by TDP-43, suggesting a multitude of possible disease mechanisms (Tollervey et al., 2011; Sendtner, 2011; Polymenidou et al., 2011).

In mice TDP-43 is essential for embryogenesis (Kraemer et al., 2010; Sephton et al., 2010; Wu et al., 2010) and *TDP-43* haploinsufficiency causes a paralytic phenotype (Kraemer et al., 2010). Postnatal knockout of mouse *TDP-43* results in a dramatic loss of body fat, suggesting a metabolic function for TDP-43 (Chiang et al., 2010), and targeted depletion of mouse TDP-43 in motor neurons leads to an ALS-like neurodegenerative phenotype (Wu et al., 2012). Overexpression of *TDP-43* in mice induces neuronal loss in a dose-dependent manner and results in altered distributions of Gemini of coiled bodies and mitochondria in motor neurons (Wils et al., 2010; Shan et al., 2010; Lagier-Tourenne et al., 2010). In zebrafish, overexpression and knockdown of *TDP-43* cause swimming defects and motor neuron axonal phenotypes (Kabashi et al., 2010). In *Drosophila*, both gain and loss of *TDP-43* (*dTDP-43*) cause pupal lethality and reduced adult viability, impaired larval locomotor activity, axonal loss, and altered synaptic boutons (Wang et al., 2011; Lin et al., 2011; Ritson et al., 2010; Li et al., 2010; Feiguin et al., 2009). Although these in vivo studies show that both gain and loss of *TDP-43* can lead to a variety of neuronal defects, the underlying pathogenic mechanisms are not known.

Here, we have combined deep RNA sequencing, in silico gene network analysis, and classical *Drosophila* genetics to show that dTDP-43 is a crucial regulator of ecdysone receptor (EcR)-dependent gene network switching at the pupal-to-adult transition. Our data indicate that neuronal gain or loss of dTDP-43 strongly upregulates the expression of the neuronal

microtubule-associated protein Map205, which leads to aberrant cytoplasmic accumulation of EcR, disrupted EcR signaling, apoptosis of bursicon neurons, and failure to correctly complete the last step of metamorphosis. Because loss of the EcR homolog in mice, liver X receptor β (LXRβ), results in TDP-43-positive motor neuron degeneration (Kim et al., 2008; Bigini et al., 2010), our study suggests that LXR signaling might be disrupted in human TDP-43 proteinopathies. We propose that TDP-43-mediated neurotoxicity is the result of a loss of its normal function.

RESULTS

Gain or Loss of *dTDP-43* Leads to Immature Phenotypes Due to Defects of CCAP/Bursicon Neurons at Adult Commitment

To study the neuronal function of *dTDP-43*, we overexpressed and silenced *dTDP-43* in the fly nervous system. Both resulted in immature-looking adult escapers with unexpanded wings, soft cuticle, unretracted ptilinum, a dimpled dorsal thorax, and misoriented scutellar bristles (Figures 1A–1E). Knockdown or overexpression of *dTDP-43* in motor neurons resulted in the same immature phenotypes (Table 1). Wing expansion and cuticle hardening in *Drosophila* are posteclosion events regulated by the secretion of the insect neurohormone bursicon by a subset of 14 crustacean cardioactive peptide (CCAP)-expressing neurons in the ventral nerve cord (Luan et al., 2006). Targeted ablation of CCAP/bursicon neurons leads to pupal lethality with adult escapers showing immature cuticle and wing expansion phenotypes (Park et al., 2003). Knockdown and overexpression of *dTDP-43*, specifically in CCAP/bursicon neurons, resulted in similar phenotypes, ranging from pupal lethality to adult escapers with varying degrees of wing inflation phenotypes (Table 1). Culture temperature correlated with phenotypic severity and overexpression of *dTDP-43* caused more severe phenotypes than *dTDP-43* knockdown (Table 1). The observed *dTDP-43*-induced immature phenotypes are thus explained by defects at the level of CCAP/bursicon neurons.

Gain or Loss of *dTDP-43* Leads to Apoptosis of CCAP/Bursicon Neurons

In order to further define the nature of the CCAP/bursicon neuronal defects, we expressed the membrane marker mCD8-GFP in CCAP/bursicon neurons to visualize possible morphological defects caused by altered *dTDP-43* expression. During metamorphosis, CCAP/bursicon neurons undergo strong EcR-dependent remodeling (Zhao et al., 2008). Pruning of larval structures occurs within the first 30 hr after puparium formation (APF), whereas outgrowth of adult neurites is completed at 60 hr APF (Zhao et al., 2008). Knockdown or overexpression of *dTDP-43* did not affect the morphology or number of CCAP neurons in third instar larvae or in pupae up to 60 hr APF (Figure 2A; Figure S1), and outgrowth of adult neurites was normal at 60 hr APF (Figures 1F–1H). However, at 72 hr APF and in newly eclosed adults, the number of CCAP/bursicon neurons was reduced in both loss and gain of *dTDP-43* flies (Figure 2A). These results suggest that both increased and decreased expression of *dTDP-43* cause immature phenotypes by late pupal neuronal loss after normal metamorphic remodeling.

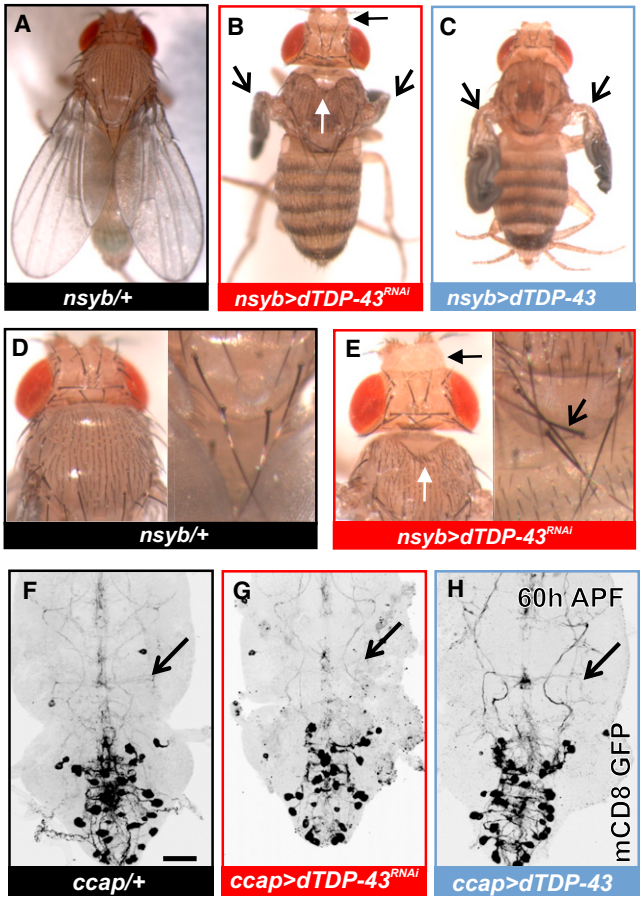

Figure 1. Neuronal Gain or Loss of *dTDP-43* Expression Causes Wing Expansion Phenotypes Due to Defects of CCAP/Bursicon Neurons

(A–E) Compared to control flies (A and D), panneuronal knockdown and overexpression of *dTDP-43* leads to phenotypes including unexpanded wings (open black arrows in B and C), dimpled thorax (white arrows in B and E), unretracted ptilinum (closed black arrows in B and E), and misoriented scutellar bristles (open black arrow in E).

(F–H) Adult neurite extension in CCAP/bursicon neurons at 60 hr APF is normal upon CCAP/bursicon neuron-specific knockdown (G) or overexpression (H) of *dTDP-43* compared to control flies. Scale bar, 50 μm.

See also Figure S1.

Because neurodegeneration in human ALS and FTD patients is characterized by ubiquitin-positive neuronal inclusions, we stained CCAP/bursicon neurons with altered dTDP-43 expression using antibodies directed against dTDP-43 and ubiquitin. We observed ubiquitin- and dTDP-43-positive accumulations in the nucleus, perinuclear region, and the cytoplasm of ~80% of dTDP-43 overexpressing CCAP/bursicon neurons. Ubiquitin-positive inclusions were not observed in dTDP-43-depleted CCAP/bursicon neurons (Figure 2B). Ubiquitin- and dTDP-43-positive accumulations were most clearly visible in dTDP-43 overexpressing neurons that were characterized by abnormal cellular and nuclear morphology likely reflecting end-stage cell

Table 1. Knockdown and Overexpression of *dTDP-43* in All Neurons, Motor Neurons, or CCAP/Bursicon Neurons at Different Culture Temperatures Cause the Same Phenotypes

	18°C		25°C		29°C	
Neuronal population (driver)	*dTDP-43^{RNAi}*	*dTDP-43*	*dTDP-43^{RNAi}*	*dTDP-43*	*dTDP-43^{RNAi}*	*dTDP-43*
Panneuronal (C155)	mild W	W	W	W	W	L
Panneuronal (nsyb)	mild W	W	W	SL + W	W	L
Motor neurons (D42)	nd	nd	W	W	nd	nd
CCAP/bursicon neurons (ccap)	no W	W	mild W	W	mild W	L

W, wing inflation phenotype; SL, late pupal semilethality (most of the pupae die between 73–90 hr APF, occasional adult escapers); L, late pupal lethality (100% of the pupae die between 73–90 hr APF, no adult escapers); nd, not done.

death (Figure 2B). Expression of apoptosis inhibitors *p35* or *DIAP1* in CCAP/bursicon neurons with increased or decreased *dTDP-43* expression rescued the CCAP/bursicon neuronal loss and wing inflation defects (Figure 2C; Figure S2). Together, these results indicate that both increased and decreased expression of *dTDP-43* cause immature phenotypes by enhanced apoptotic cell death of CCAP/bursicon neurons starting at 72 hr APF. Our data also suggest that formation of ubiquitin- and dTDP-43-positive inclusions is not a prerequisite for dTDP-43-mediated neurotoxicity in CCAP/bursicon neurons.

Gain and Loss of *dTDP-43* Cause Significantly Overlapping Transcriptome Alterations

To identify molecular pathways underlying the specific late pupal neurodegenerative phenotypes, we sequenced transcriptomes of heads with altered *dTDP-43* expression at the developmental stage when the CCAP/bursicon neuronal defect was observed (73–90 hr APF; Gene Expression Omnibus [GEO] accession number GSE42844). Pupae overexpressing *dTDP-43* were generated by crossing the ubiquitous *act5c-GAL4* driver to *UAS-dTDP-43-Flag* (*dTDP-43^{GOF}*) (Figure S3A), resulting in moderately increased *dTDP-43* transcript and protein levels (Figures S3B and S3C). To produce pupae with ubiquitously decreased *dTDP-43* expression, we used transheterozygous combinations of *dTDP-43$^{\Delta 23}$* and *dTDP-43$^{\Delta 142}$*, two reported mutants (Feiguin et al., 2009) *and Df(2R)106*, a deficiency uncovering *dTDP-43* (Figure S3D). For differential gene expression analysis, sequencing data of the transheterozygous *dTDP-43$^{\Delta 23/\Delta 142}$* and *dTDP-43$^{\Delta 142/Df(2R)106}$* genotypes were pooled (*dTDP-43^{LOF}*). A statistically significant overlap was observed between *dTDP-43^{LOF}* and *dTDP-43^{GOF}* for the upregulated and downregulated sets of transcripts (Figures 3A and 3B; Tables S1, S2, S3, and S4; Figure S3E). Because we prepared cDNA libraries from rRNA-depleted total RNA samples, our data also allowed differential expression analysis of noncoding RNAs. Interestingly, 17% and 15% of the upregulated genes in *dTDP-43^{GOF}* and *dTDP-43^{LOF}* flies, respectively, corresponded to small nucleolar RNA genes (snoRNAs), which again significantly overlapped between the two genetic conditions (Figure 3B). Finally, we looked if dTDP-43 affected transcript splicing and found 206 and 176 genes in *dTDP-43^{GOF}* and *dTDP-43^{LOF}* flies, respectively, that showed different sets of expressed transcripts compared to controls. Again, we observed statistically significant overlap between the two conditions (Figure 3B; Table S5).

Next, we searched for enriched Gene Ontology (GO) annotations in the set of genes that were commonly up- or downregulated in *dTDP-43^{GOF}* and *dTDP-43^{LOF}* flies. The highest enrichment scores for both the up- and downregulated gene sets were found for clusters related to the chitin-based cuticle (Figure 3C). Among the downregulated genes, additional clusters referred to the mitochondrial respiratory chain and the muscular actin-myosin cytoskeleton (Figure 3C). Genes that showed altered splicing patterns in *dTDP-43^{GOF}* and *dTDP-43^{LOF}* flies were significantly enriched for a cluster related to axonal growth (Figure 3C).

Together, these data showed that, in line with our phenotypic observations, decreased and increased *dTDP-43* resulted in highly similar transcriptome alterations at the level of coding and noncoding RNA during late pupal stages. The results also highlighted a specific role for *dTDP-43* in snoRNA processing, mRNA splicing, mitochondrial respiration, actin-myosin dynamics, axonal growth, and cuticle deposition in late metamorphosis.

Gain or Loss of *dTDP-43* Results in a Failure of EcR to Switch Off the *br*-Mediated Pupal Transcriptional Program

Because the dTDP-43-mediated phenotypes originated at late pupal stages, we wondered if *dTDP-43^{LOF}* and *dTDP-43^{GOF}* disrupted specific developmental gene networks during metamorphosis. We therefore looked at the wild-type modEncode developmental time course transcription profiles (Graveley et al., 2011) of all commonly up- and downregulated genes in *dTDP-43^{LOF}* and *dTDP-43^{GOF}* late pupae and ranked them according to their fold change in expression. A large fraction of the upregulated genes had developmental expression patterns that peak during late larval/early pupal stages and are repressed at the end of metamorphosis (Figure 4A). Conversely, the downregulated gene set was enriched for genes that are typically switched-on in late pupal stages (Figure 4A). These data demonstrate that *dTDP-43^{LOF}* and *dTDP-43^{GOF}* cause a failure to switch gene expression from a pupal to an adult pattern in late metamorphosis, in line with the immature adult phenotypes and late pupal lethality.

To further explore this disrupted metamorphic gene network, we used the integrated target and enhancer prediction tool i-*cis*Target to check if the genomic regions of differentially expressed genes were enriched for specific clusters of transcription factor binding sites modeled by a position weight matrix

(PWM) (Aerts et al., 2010; Herrmann et al., 2012). In the list of upregulated genes we identified 151 out of 6,383 tested PWM motifs with an enrichment score (E-score) above 2.5 (Table S6). The list contained three highly similar motifs: 5′-CAAGGTC-3′ (ranked first, E-score: 4.75), 3′-GAAGGTCA-5′ (ranked tenth, E-score: 4.27), and 5′-AAGGTCA-3′ (ranked 54th, E-score: 3.30). The latter two corresponded to the recognition motifs of the nuclear hormone receptors Hr39 and the estrogen-related receptor (ERR) and strongly resemble the archetypical AGGTCA half-site consensus motif for nuclear hormone receptors, including EcR (King-Jones and Thummel, 2005) (Figure 4B; Table S6). Next, we used i-*cis*Target to detect enrichment of experimentally validated in vivo transcription factor binding sites (derived from modENCODE ChiP-seq data) and retrieved five hits of which two corresponded to EcR (Table S7). EcR binding regions were identified in 44 significantly highly ranked genomic regions of which nine were located upstream of the transcription factor *broad* (*br*), a key mediator of ecdysone signaling. Because of the upregulation of *br*, the identification of predicted and experimentally validated EcR binding sites and because expression levels of EcR or its heterodimeric partner Usp were not altered (Table 2), our results indicated a gene network disruption downstream of the nuclear steroid receptor EcR. In line with this notion, the ten genes from the *L71* gene cluster, which are normally induced directly by br only in prepupae (Crossgrove et al., 1996), were strongly expressed in the *dTDP-43^{LOF}* and *dTDP-43^{GOF}* late pupae (Table 2).

During metamorphosis br acts as a pupal specifier, and its switching-off by ecdysone at adult commitment is required to change cuticle gene expression from the pupal to the adult program (Zhou and Riddiford, 2002). Supporting a specific disruption of this process, the larval-specific (*Lcp65Ag2*, *Lcp4*, *Lcp65Ad*) and early pupal cuticle genes (*Edg84A*, *PcP*, *Edg91*, *Edg78E*) were not yet switched-off, whereas the well-characterized adult cuticle gene *Acp65Aa* was not sufficiently induced in late pupal *dTDP-43^{LOF}* and *dTDP-43^{GOF}* flies (Table 2). These results demonstrate that dTDP-43 dysfunction results in the inappropriate continuation of the br-mediated pupal transcriptional program due to the failure of EcR to switch it off.

Gain or Loss of *dTDP-43* Causes Cytoplasmic EcR-A Accumulations in CCAP/Bursicon Neurons

Next, we wondered if dTDP-43 dysfunction also disrupted EcR function in the CCAP/bursicon neurons. EcR plays an important role in metamorphic neuronal remodeling, including the CCAP/bursicon neurons (Zhao et al., 2008). EcR codes for three protein isoforms, of which EcR-A and EcR-B1 are predominantly expressed in the central nervous system. At the start of metamorphosis most larval neurons express EcR-B1 when they lose their larval features, whereas EcR-A is the predominant isoform in late metamorphosis (Truman et al., 1994). We observed that EcR-A is expressed at low levels in CCAP/bursicon neurons (Figure 4C). Interestingly, in CCAP/bursicon neurons in which dTDP-43 was up- or downregulated, EcR-A accumulated in the neuronal cytoplasm. These data suggest that increased or decreased dTDP-43 affects EcR signaling by controlling EcR subcellular distribution.

EcR is the ortholog of the mammalian liver X receptors (LXR) (Figure S4A), and loss of LXR function is associated with neuronal degeneration in mice (Andersson et al., 2005; Bigini et al., 2010; Kim et al., 2008; Wang et al., 2002). Interestingly, we obtained evidence for functional (Figure S4B) and physical (Figures S4C–S4E) interactions between TDP-43 and LXR, suggesting that the TDP/LXR link might be functionally conserved in mammals (see the Discussion).

dTDP-43 Binds to *Map205* mRNA and Controls Its Transcript Levels to Regulate the Subcellular Distribution of EcR

The most significantly upregulated gene in *dTDP-43^{GOF}* and *dTDP-43^{LOF}* flies was Map205 (Figures 3A and 5A; Figure S5A). Map205 is a PAM2 motif (Albrecht and Lengauer, 2004) containing neuronal microtubule binding protein (Rolls et al., 2007). Map205 has no mammalian sequence homologs but is functionally and structurally related to mammalian MAP4 (Pereira et al., 1992). Because the developmental expression profile of *Map205* did not follow the dynamic pattern of EcR-responsive genes like *br* (Figure 4A), we hypothesized that *dTDP-43*-mediated *Map205* overexpression acted upstream of EcR and that dTDP-43 might bind directly to *Map205* RNA. RNA immunoprecipitation (RIP) revealed that dTDP-43 bound to its own and *Map250* mRNA but not to mRNA of the synaptotagmin genes *Syt*α or *Syt*β, two presynaptic genes whose expression was not significantly altered in our trancriptome analysis (Figure 5B). In addition, neuron-specific silencing of *Map205* in *dTDP-43^{LOF}* mutants strongly suppressed the late pupal lethality resulting in escaper frequencies close to the Mendelian fraction expected for full rescue (Figure S5C) as well as the immature wing inflation phenotypes induced by panneuronal knockdown and overexpression of *dTDP-43* (Figure S5F). *Map205* RNAi-mediated rescue was caused by efficient *Map205* knockdown (Figure S5D) and is not explained by GAL4 dilution effects induced by multiple UAS-constructs in the background (Figure S5E). CCAP/bursicon neuron-specific knockdown of *Map205* also suppressed the wing inflation phenotypes (Figure S5B) and the loss of bursicon neurons (Figure 5C). Finally, cytoplasmic EcR-A accumulations in CCAP/bursicon neurons with altered *dTDP-43* expression decreased significantly when *Map205* was downregulated (Figures 5D and 5E). Together, these data support a model in which dTDP-43 controls Map205 expression levels by directly binding to Map205 mRNA to regulate the normal cellular distribution of EcR and hence proper EcR signaling.

DISCUSSION

A Function for dTDP-43 in Map205-Dependent EcR-Dependent Transcriptional Program Switching, Metamorphosis, and Neuronal Survival

Despite the expected wide range of biological functions and pathogenic mechanisms of TDP-43 (Sendtner, 2011), we identified a specific neuronal function of *dTDP-43* explaining its essential role during late metamorphosis and early adult maturation in *Drosophila* (Feiguin et al., 2009; Hanson et al., 2010; Lin et al., 2011). We show that dTDP-43 is a crucial regulator of the survival of the CCAP/bursicon neuronal network, whose main function is

Cell PRESS
Open ACCESS

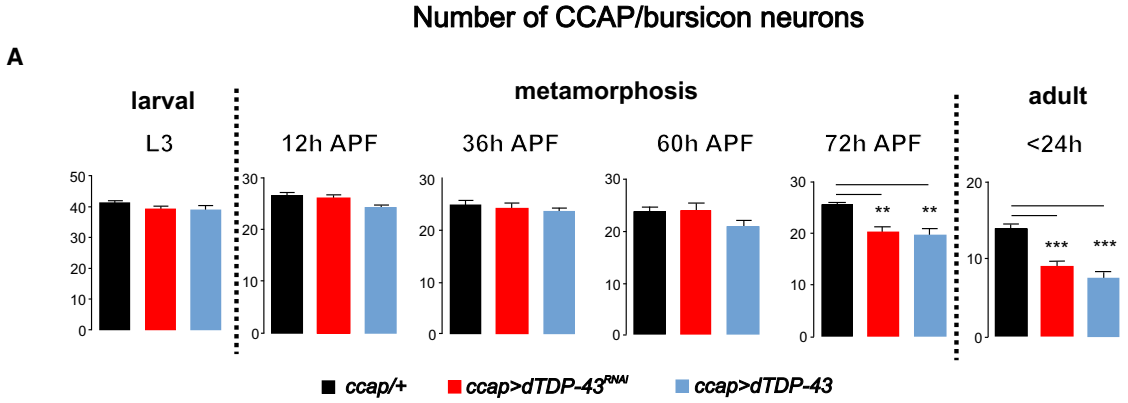

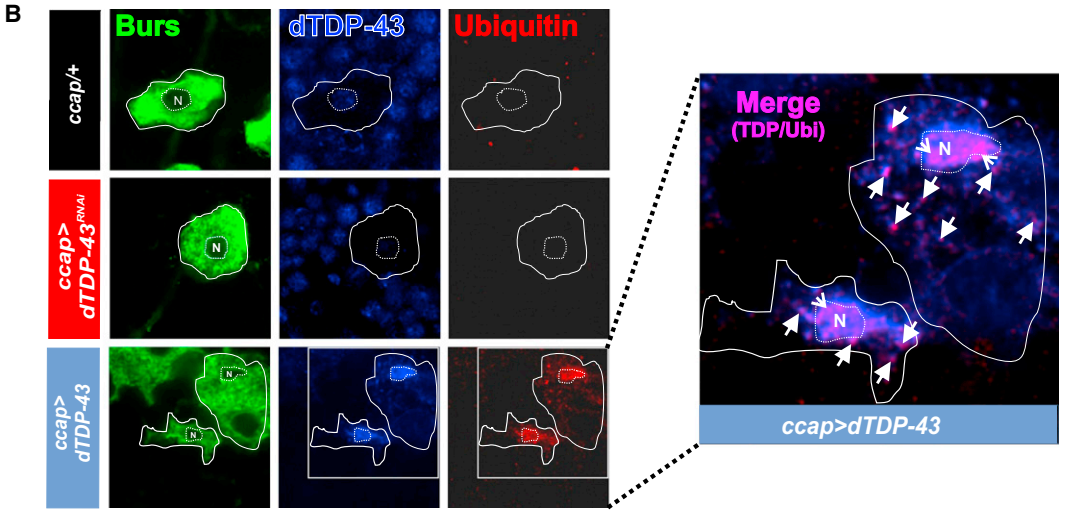

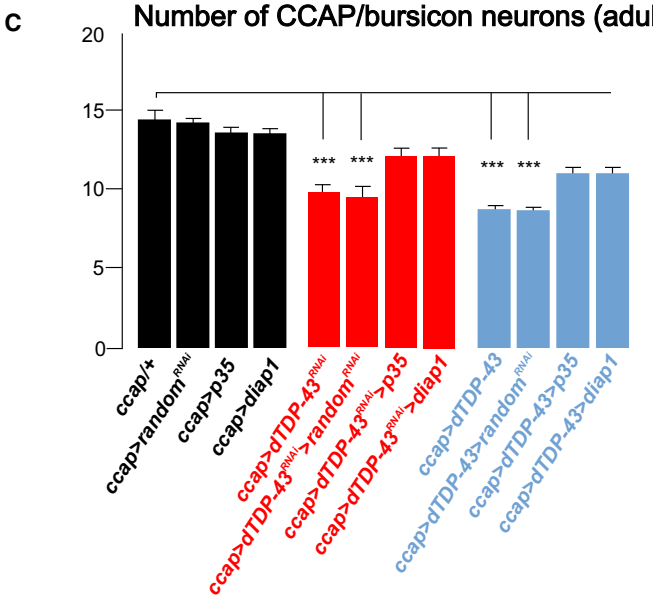

(legend on next page)

to coordinate the pupal-to-adult transition (Park et al., 2003). In addition, deep RNA sequencing of *dTDP-43* gain and loss-of-function mutants revealed that dTDP-43 regulates *EcR-br*-dependent transcriptional network switching from a pupal to an adult-specific pattern, thereby providing a molecular basis for the late-pupal lethality and immature adult cuticle and wing inflation phenotypes. Interestingly, we demonstrate that dTDP-43 mediates these functions by directly binding to *Map205* mRNA to control *Map205* expression, which in turn mediates EcR subcellular localization and signaling. Because it has been suggested that EcR nucleocytoplasmic shuttling depends on the microtubule network (Vafopoulou, 2009), Map205 might over- or destabilize microtubules, resulting in cytoplasmic accumulation of EcR. Regardless of the exact mechanism, our study establishes dTDP-43 as a crucial regulator of steroid hormone receptor-mediated transcriptional program switching, which is central for its function in neuronal survival and pupal-to-adult transformation.

TDP-43, Nuclear Hormone Signaling, and Neurodegenerative Disease

Although these findings indicate an important biological function for dTDP-43 during the final stages of *Drosophila* metamorphosis, they are relevant in the context of human neurodegenerative disease for several reasons. First, we found that dTDP-43 dysfunction disrupts pupal-to-adult transformation by inducing apoptotic cell death rather than defective developmental proliferation or remodeling of CCAP/bursicon neurons. This suggests that, in line with the adult-onset of human neurodegenerative TDP-43 proteinopathies, an evolutionary conserved function of TDP-43 may be to maintain postdevelopmental neuronal integrity. Second, it is intriguing that the CCAP/bursicon neuronal network, a very specific and small subset of neurons in the *Drosophila* ventral nerve cord, the homologous structure of the vertebrate spinal cord, is particularly vulnerable to dTDP-43 dysfunction. This is reminiscent of the neuronal selectivity seen in ALS and FTD and suggests that *Drosophila* might be a useful model to study the underlying mechanisms of selective neuronal vulnerability, a major unresolved topic in the human neurodegenerative disease field (Saxena and Caroni, 2011). Third, it is of interest that mutational inactivation of the mouse *EcR* homologs, *LXR-*α and *-*β, has been reported to cause neuronal degeneration and that loss of mouse *LXR-*β causes causes TDP-43-positive motor neuron degeneration (Andersson et al., 2005; Bigini et al., 2010). Further supporting a role for disrupted LXR signaling in TDP-43 proteinopathy, we here report that the LXR recognition motif was significantly enriched among genes that have been recently reported to be upregulated in TDP-43-depleted mouse brain (Polymenidou et al., 2011) and that LXR and TDP-43 colocalized and physically interacted in human neuronal cell lines (Figure S4). Interestingly, nuclear hormone receptor signaling has also been implicated in the X-linked human motor neuron degenerative disorder spinal and bulbar muscular dystrophy, which is caused by a polyglutamine tract expansion in the nuclear androgen receptor whose native functions are likely essential to pathogenesis (Nedelsky et al., 2010).

TDP-43 Neurotoxicity: Toxic Gain or Loss of Normal Function?

Our discovery in *Drosophila* that dTDP-43 plays a major role in Map205-EcR-br-dependent transcriptional program switching and survival of CCAP/bursicon neurons, allowed us to shed some light on the question of whether TDP-43 neurotoxicity in ALS and FTD is mediated by a loss of its normal function or by an unrelated toxic GOF mechanism triggered by misfolded/aggregated TDP-43 (Lee et al., 2011). Although we found that upregulation of *dTDP-43* seemed to be able to induce neuronal ubiquitin- and dTDP-43-positive inclusions, it is not clear if they represent true misfolded/aggregated dTDP-43 because further corroborative biochemical evidence is lacking. However, both up- and downregulated *dTDP-43* resulted in virtually identical phenotypes, including specific apoptotic loss of CCAP/bursicon neurons, cytoplasmic EcR accumulations, highly similar transcriptome alterations, and a specific disruption of Map205-EcR-br signaling. These data suggest that dTDP-43 LOF is sufficient to induce neuronal cell death and that dTDP-43 overexpression results in its own LOF. Therefore, the formation of ubiquitin- and dTDP-43-positive inclusions is not required to induce neuronal cell death. Although the exact mechanism by which increased dTDP-43 expression results in its LOF remains to be established, our data showing that dTDP-43 strongly binds to mRNA of *Map205*, which controls EcR signaling, suggest that disruption of this binding by altered dTDP-43 expression is at the heart of this process. dTDP-43 overexpression might lead to a loss of its normal function by disturbing the stoichiometric balance of the TDP-43 containing functional protein complex (Freibaum et al., 2010; Sephton et al., 2011) possibly in a dominant-negative manner as has been shown previously for disrupted Notch signaling by presenilin overexpression in *Drosophila* (Ye and Fortini, 1999). Regardless of the underlying mechanism, our study indicates that dTDP-43 neurotoxicity is more likely caused by a loss of its normal function than by a toxic property

Figure 2. Neuronal Gain or Loss of *dTDP-43* Causes Postdevelopmental Apoptosis of CCAP/Bursicon Neurons

(A) Number of CCAP/bursicon neurons with decreased (*ccap* > *dTDP-43*^{RNAi}) or increased (*ccap* > *dTDP-43*) dTDP-43 expression is normal in L3 larvae and in pupae up to 60 hr APF. Enhanced CCAP/bursicon neuronal loss is observed in late pupae 72 hr APF and young adult flies. APF, after puparium formation. One-way ANOVA with post hoc Dunn's test: **p $\leq$ 0.01 ***p $\leq$ 0.001, n = 10 for each genotype. Error bars represent SEM.

(B) CCAP/bursicon neuron-specific dTDP-43 overexpression (*ccap* > *dTDP-43*) but not knockdown (*ccap* > *dTDP-43*^{RNAi}) induces nuclear and cytoplasmic ubiquitin- and dTDP-43-positive inclusions. To avoid oversaturation of the dTDP-43 signal in *ccap* > *dTDP-43* a laser intensity of 75% compared to other genotypes was used. Bursicon staining (green) was used to label CCAP/bursicon neurons. dTDP-43 is labeled in blue. Ubiquitin is labeled in red. dTDP-43/ubiquitin colabeling is in magenta. N indicates the nucleus. Closed arrows indicate cytoplasmic ubiquitin/dTDP-43-positive accumulations. Open arrows indicate nuclear and perinuclear ubiquitin/dTDP-43-positive accumulations.

(C) CCAP/bursicon neuron-specific expression of apoptosis inhibitors *p35* and *DIAP1* suppresses the immature wing inflation phenotypes induced by knockdown (*ccap* > *dTDP-43*^{RNAi}) and overexpression (*ccap* > *dTDP-43*) of *dTDP-43*.

See also Figure S2.

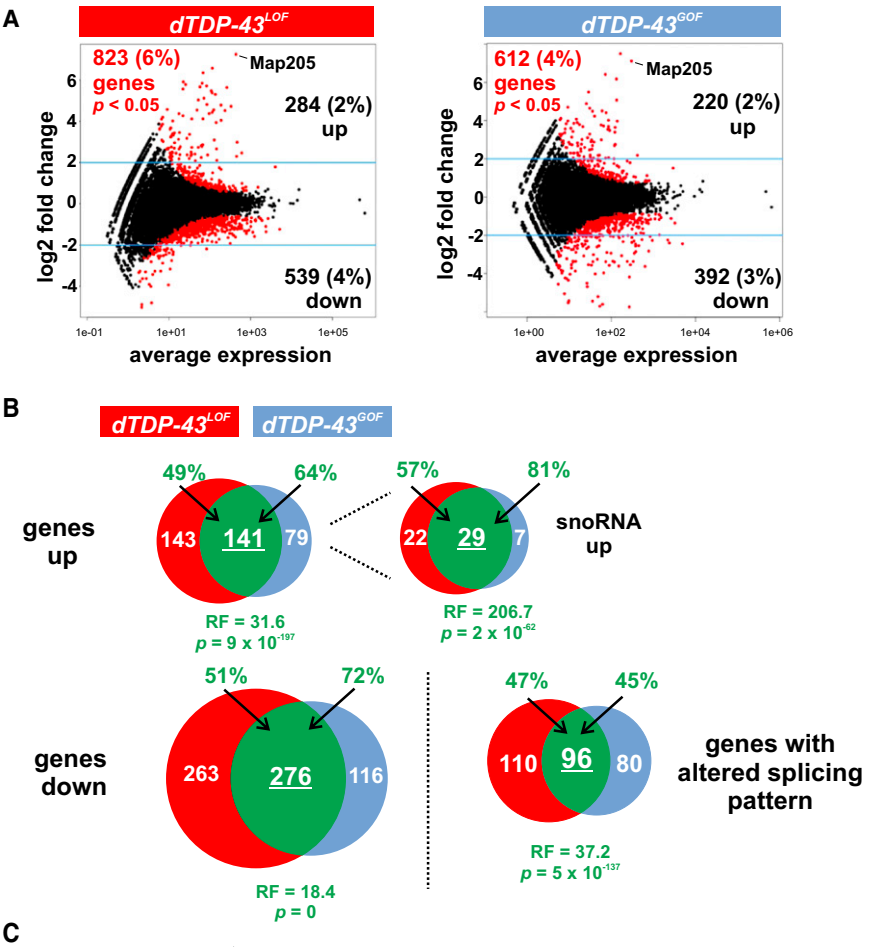

C

	DAVID Annotation Clusters	Enrichment Score (>2.5)
genes up	Insect cuticle	5.4
genes down	Insect cuticle	22.1
	Mitochondrial respiratory chain	7.3
	Muscle myosin/actin	3.3
altered splicing	Axonal growth	2.8

Figure 3. RNA-Seq Analysis of Loss and Gain of *dTDP-43* Expression Results in Overlapping Sets of Differentially Expressed Genes

(A) Scatter plot of log2 fold change versus mean comparing *dTDP-43*^{LOF} and *dTDP-43*^{GOF} with controls. Total number of differentially expressed genes (in red), upregulated genes, downregulated genes, and Map205 are indicated for both genetic conditions.

(B) Area-proportional Venn diagrams indicating the degree of overlap between *dTDP-43*^{LOF} and *dTDP-43*^{GOF} for upregulated and downregulated genes and genes with altered splicing pattern. RF, representation factor.

(C) DAVID Gene Ontology annotation analysis in commonly upregulated and downregulated genes and genes with altered splicing patterns in *dTDP-43*^{LOF} and *dTDP-43*^{GOF}.

See also Tables S1, S2, S3, S4, S5, and Figure S3.

of misfolded/aggregated protein that is independent of its native function. Interestingly, our conclusion is supported by a recent study in mouse in which targeted depletion of TDP-43 in lower motor neurons resulted in postdevelopmental ALS-like phenotypes, including amyotrophy, motor neuron loss, microglial activation, and astrocytosis (Wu et al., 2012).

Our observation of strongly overlapping transcriptome alterations upon increased and decreased dTDP-43 levels seems at odds with a recently published RNA-seq study in *Drosophila* showing largely nonoverlapping transcriptome alterations upon up- and downregulation of dTDP-43 (Hazelett et al., 2012). However, libraries generated in this study were extracted from dissected central nervous systems of third instar larvae, whereas we isolated RNA from late pupal complete heads. This difference is important as the EcR signaling defect we observed appears to be specific to the pupal-adult transition. In addition, the libraries from complete heads contained a large number of cuticle genes that turned out to be highly informative in identifying the EcR signaling defect.

In conclusion, we propose a model in which neurodegeneration is caused by the loss of the normal function of dTDP-43 in *Drosophila*. dTDP-43 acts as a central coordinator of a four-step molecular pathway involved in the regulation of gene networks, neuronal survival, and adult maturation: (1) dTDP-43 dysfunction directly upregulates the expression of the neuronal microtubule binding protein Map205; (2) Map205 overexpression leads to aberrant cytoplasmic accumulation of nuclear EcR; (3) disrupted EcR signaling causes a failure to switch gene networks from a pupal to adult pattern; and (4) failure of EcR-dependent gene network switching leads to neuronal apoptosis of bursicon neurons and renders flies unable to complete the final maturation step at the pupal-to-adult transition. Our study lends further support to the view that a loss of normal TDP-43 function rather than a novel toxic GOF constitutes the pathogenic mechanism in human TDP-43 proteinopathies.

EXPERIMENTAL PROCEDURES

Drosophila Stocks

D. melanogaster strains were maintained on standard yeast, cornmeal, and agar-based medium, and test crosses were performed at 25°C unless noted otherwise. The w^{1118} (Canton-S10) line was used as wild-type

control. RNAi stocks *v39690* (*Map205^{RNAi}*), *v100307* (*random^{RNAi} against* CG7946), and *v104401* (*dTDP-43^{RNAi}*) were obtained from the Vienna *Drosophila* RNAi center (VDRC). *Df(2R)106*, *P{UAS-p35.H}BH1*(UAS-p35), *P{UAS-DIAP1.H}3* (UAS-DIAP1), and GAL4 driver lines *P{Act5C-GAL4}25FO1* (*act5C-GAL4*), *P{GD4553}* (*nsyb-GAL4*), *P{GawB}elav[C155]* (*c155-GAL4*), and *P{GawB}D42* (*D42-GAL4*) were obtained from the Bloomington Stock center. The *ccap-GAL4*, *UAS-mCD8-GFP* stock was kindly provided by Randall S. Hewes. *dTDP-43$^{\Delta 23}$*, *dTDP-43$^{\Delta 142}$*, and *UAS-dTDP-43-Flag* flies were a gift from Fabian Feiguin, and the *dTDP-43^{null}* allele was provided by Fabienne Fiesel.

Immunohistochemistry

Immunostaining on central nervous system was performed using standard techniques. The following primary antibodies were used: mouse monoclonal mouse anti-EcR-A (Development Studies Hybridoma bank) at 1:10, mouse anti-ubiquitin (Cell Signaling Technology, Danvers, MA, USA) at 1:400, rabbit anti-GFP (Invitrogen, Carlsbad, CA, USA) at 1:500, and rabbit anti-dTDP-43 at 1:3000 and anti-Bursicon α (kindly provided by Benjamin White) at 1:5,000. Secondary antibodies conjugated to FITC, Cy3, or Cy5 were used at 1:200 (Jackson ImmunoResearch, Reston, VA, USA). Ventral nerve cords were mounted in Vectashield mounting medium (Vector Laboratories, Burlingame, CA, USA) and analyzed with a Fluoview FV1000 confocal microscope (Olympus). Images of multiple fluorescent-labeled ventral nerve cords were obtained by sequential scanning of each channel at equal laser intensity unless noted otherwise. For the CCAP/bursicon neuron counts, we stained and counted the amount of cell bodies of ten ventral nerve cords. The experimenter was blinded to genotype. One-way ANOVA was used to evaluate significant variation among genotypes; a post hoc Dunns test was used for the CCAP/bursicon neuron counts to assess the contribution of each genotype. For the bursicon neuron counts, a post hoc Bonferroni's Multiple Comparison Test was performed.

Image Quantification

To measure EcR cytoplasmic/nuclear ratios in CCAP/bursicon neurons, ImageJ Software was used to measure the fluorescence intensity (mean gray values) of confocal images. Images were made with equal laser intensity unless noted otherwise with a Fluoview FV1000 confocal microscope (Olympus). Ten CCAP/bursicon neurons of different VNCs were analyzed. Mean gray values of nucleus and cytoplasma were measured and the cytoplasmic versus nuclear intensity ratio was calculated. Statistical analysis was done using one-way ANOVA with post hoc Bonferroni's multiple comparison test.

Immunoblotting

Twenty fly heads were homogenized on ice in radioimmune precipitation buffer (RIPA: 0.1% sodium dodecyl sulfate [SDS], 150 mM NaCl, 0.5% Na, 1% NP-40, 50 mM Tris-HCl [pH 8.0]) supplemented with protease inhibitor (Complete Protease inhibitor, Roche, Indianapolis, IN, USA). Homogenates were incubated on ice for 20 min, sonicated, and cleared at 14,000 rpm for 20 min at 4°C. Supernatants were used for immunoblotting. By bicinchoninic acid colorimetric (BCA) assay (Perbio Science N.V.) protein concentrations were measured. Twenty micrograms of protein was separated on a 10% Nupage Bis-Tris gels (Invitrogen) and blotted onto a polyvinylidene difluoride (PVDF) membrane. Membranes were blocked in 5% skimmed milk in PBS containing 0.1% Tween20 (Merck, Whitehouse, NJ, USA) and probed with primary antibody (rabbit anti-dTDP-43 [1:12,000] and rat anti-elav 7E8A10 (Developmental Studies hybridoma bank) [1:2,000]). Immunodetection was performed with specific secondary antibodies conjugated to horseradish peroxidase and the ECL- plus chemiluminescent detection system (Amersham Biosciences, Little Chalfont, UK) with bands quantified on a Kodak Imaging Station 440 (Eastman Kodak, Rochester, NY, USA). The signal was normalized to the signal obtained from elav for quantification.

Library Generation and Sequencing Using AB SOLID

Total RNA was isolated in duplicate from 150 late pupal heads (73–90 hr APF) of the following genotypes: *w^{1118}*, *w^{1118}*; *act5c > dTDP-43*, *w^{1118}*; *dTDP-43$^{\Delta 23/\Delta 142}$*, and *w^{1118}*; *dTDP-43$^{\Delta 142/Df(2R)106}$*. Ribosomal RNA was removed using the RiboMinus Eukaryote Kit for RNA-seq (Invitrogen). The corresponding eight barcoded cDNA libraries were constructed using the SOLiD Whole Transcriptome Analysis and SOLiD RNA Barcoding Kits (Applied Biosystems) and sequenced on one slide using the SOLiD 3 Plus system (Applied Biosystems) at the Centre for Genomic Research (University of Liverpool, UK).

Mapping and Measurement of Gene Expression

The Bioscope Whole Transcriptome (WT) Pipeline (Applied Biosystems) was used for read mapping using default parameters. Briefly, color space reads were mapped against the complete *Drosophila melanogaster* reference genome (dm3, BDGP Release 5). After this initial mapping, this pipeline performs several additional mappings against specific sequence subsets, namely, exon junctions and exon sequences obtained from the FlyBase Release 5.12 annotations (FlyBase track from the UCSC Genome Browser). Contaminating sequences such as adapters and repeat sequences were filtered out. To count the number of reads per gene, we used the HTSeq package version 0.5.3 (function *htseq-count*) (http://www-huber.embl.de/users/anders/HTSeq/doc/overview.html), with gene annotation from *Drosophila melanogaster* FlyBase Release 5.12.

Differential Gene Expression and Splicing Analysis

Differential expression analysis between *dTDP-43^{LOF}* (four replicates) and *w^{1118}* (two replicates) and between *dTDP-43^{GOF}* (two replicates) and *w^{1118}* was performed using the Bioconductor package DESeq version 1.2.1 (R version 2.12) (Anders and Huber, 2010). DESeq first normalizes the data to correct for different library sizes and then estimates biological variability across samples and tests for differential expression based on the negative binomial distribution model. Genes are considered as differentially expressed when the Benjamini-Hochberg corrected p value is below 0.05. Overlap between gene lists was statistically evaluated by calculating the representation factor (RF) and associated probability. The RF is the number of overlapping genes divided by the expected number of overlapping genes drawn from two independent groups. An RF > 1 indicates more overlap than expected of two independent groups, and an RF < 1 indicates less overlap than expected. Probability was calculated using the exact hypergeometric probability formula.

To quantify and determine isoform abundance and isoform differential expression between *dTDP-43^{LOF}* and wild-type control and between *dTDP-43^{GOF}* and wild-type control, we used Cufflinks and Cuffdiff (Trapnell et al., 2012), with the *Drosophila melanogaster* reference annotation (*D. melanogaster* FlyBase r5.25), hence avoiding novel isoform identification. To identify genes with altered splicing pattern, we made use of the Cuffdiff output file. We selected genes with multiple alternative transcripts having at least one transcript with FC > 2 (FDR < 0.05) and at least one with FC < −2 (FDR < 0.05) in *dTDP-43^{LOF}* compared to control and in *dTDP-43^{GOF}* compared to control.

qRT-PCR

RNA was isolated from 50 heads of *w1118*, *act5c > dTDP-43*, *dTDP-43$^{\Delta 23/\Delta 142}$*, *dTDP- 43$^{\Delta 142/Df(2R)106}$*. Heads were collected in 1 ml of TRI reagent (Sigma-Aldrich, St. Louis, MO, USA) and were grounded with a plastic disposable pestle grounded. Total RNA was isolated by using standard procedures. cDNA was generated from 1 μg of RNA of each sample by using an anchored oligo(dT)18 primer and a hexamer primer according to the instructions of the Transcriptor first-strand cDNA synthesis kit (Roche). qRT-PCRs were performed on an ABI7000 instrument with qPCR Mastermix Plus for SYBR Green I (Eurogentec, San Diego, CA, USA) with primers designed by PrimerExpress software (Applied Biosystems) (see the Extended Experimental Procedures). Expression levels of transcripts from the various samples were normalized to the housekeeping genes *Rpl32*, *Rps13*, and *Gadph*.

Immunoprecipitation and RNA Identification by qRT-PCR

100 *w^{1118}* fly brains were dissected and washed three times in ice-cold PBS. The tissue was teased apart with a Dounce homogenizer followed by centrifugation for 5 min at 1,500 rpm at 4°C. The tissue was resuspended in the RIP

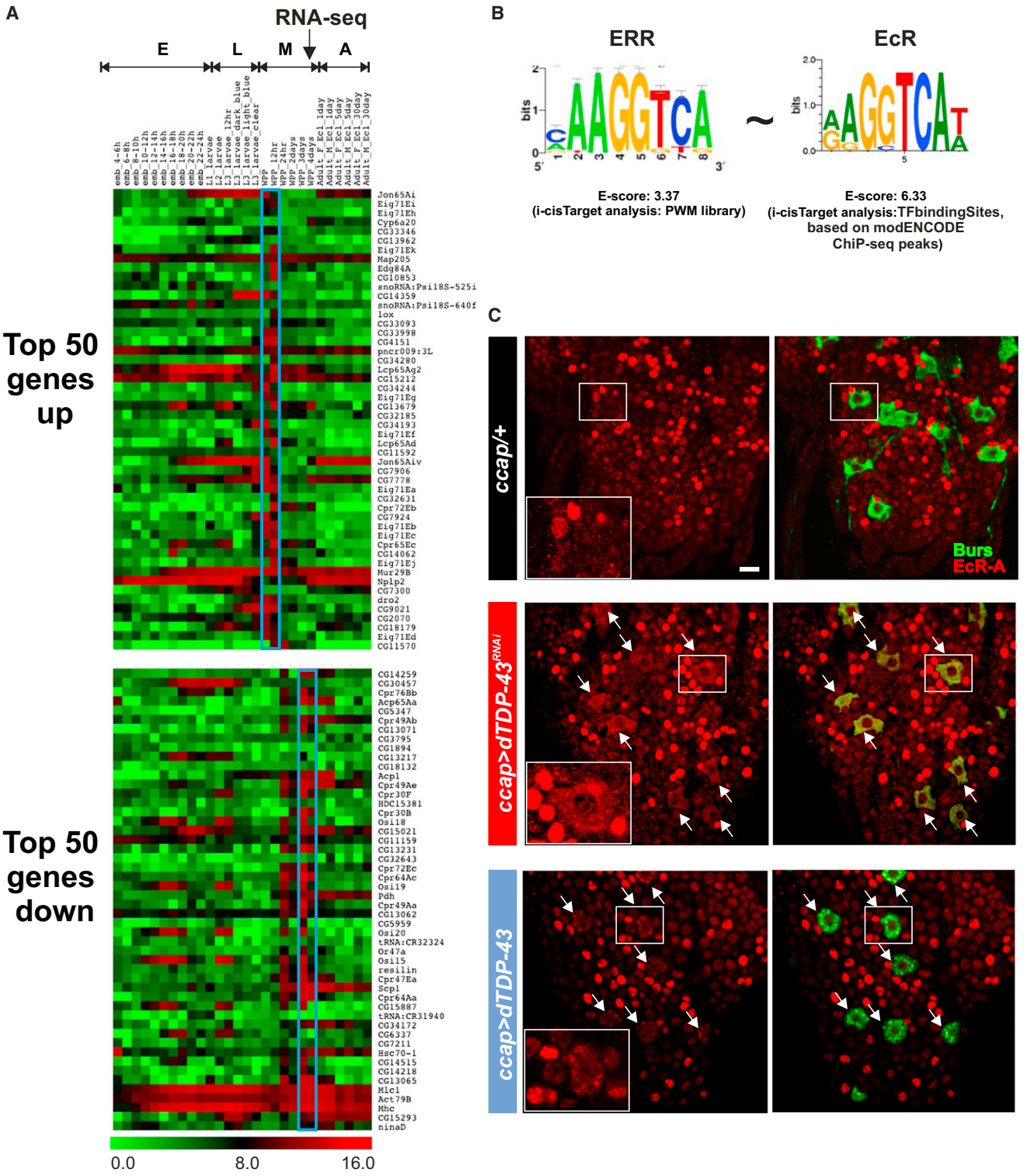

Figure 4. Loss and Gain of *dTDP-43* Result in a Failure to Switch Trancriptome Profiles from a Larval/Pupal to Adult Profile and Alter Subcellular Localization and Signaling of *EcR*

(A) Heat maps of developmental trancriptome profiles of the top 50 up- and downregulated genes in the overlapping fraction between *dTDP-43*^{LOF} and *dTDP-43*^{GOF}. E, embryonic stage; L, larval stage; M, metamorphosis; and A, adult. Blue boxes indicate early metamorphosis for the upregulated genes and late metamorphosis for the downregulated genes. The developmental time point when RNA-seq analysis was performed is indicated with an arrow.

(legend continued on next page)

Table 2. List of *dTDP-43*-Mediated Deregulated Genes Indicating Disruption of a Gene Network Downstream of *EcR* and *br*

		dTDP-43^{LOF}		*dTDP-43^{GOF}*	
Gene		log2-fold change	p Value	log2-fold change	p Value
Ecdysone receptor	*EcR*	0.31	NS	0.39	NS
Ultraspiracle	*Usp*	0.71	NS	0.50	NS
broad	*br*	1.60	1.7×10^{-9}	1.50	5.4×10^{-6}
L71 gene cluster	*Eig71Ea*	4.54	2.9×10^{-33}	3.77	2.1×10^{-15}
	Eig71Eb	3.93	9.4×10^{-31}	3.55	9.5×10^{-19}
	Eig71Ec	4.52	2.5×10^{-45}	3.48	1.3×10^{-19}
	Eig71Ed	4.43	1.3×10^{-31}	2.89	4.0×10^{-7}
	Eig71Ef	4.78	2.2×10^{-43}	4.01	1.2×10^{-21}
	Eig71Eg	5.37	1.8×10^{-36}	4.23	1.6×10^{-13}
	Eig71Eh	Inf	9.0×10^{-19}	Inf	3.7×10^{-8}
	Eig71Ei	Inf	6.2×10^{-11}	Inf	2.8×10^{-6}
	Eig71Ej	3.09	4.0×10^{-23}	3.40	1.1×10^{-22}
	Eig71Ek	6.57	6.2×10^{-42}	7.50	2.5×10^{-54}
Larval cuticle genes	*Lcp65Ag2*	4.13	8.2×10^{-13}	4.50	3.9×10^{-13}
	Lcp4	1.93	7.4×10^{-3}	2.24	5.4×10^{-3}
	Lcp65Ad	4.06	1.3×10^{-38}	3.97	2.3×10^{-29}
Pupal cuticle genes	*Edg84A*	5.68	8.5×10^{-24}	6.41	1.3×10^{-29}
	Pcp	1.43	3.2×10^{-3}	2.00	8.7×10^{-7}
	Edg91	1.27	2.0×10^{-2}	1.97	2.7×10^{-4}
	Edg78E	2.67	1.2×10^{-19}	2.76	6.4×10^{-16}
Adult cuticle gene	*Acp65Aa*	−1.63	4.5×10^{-12}	−4.16	1.2×10^{-27}

NS, not significant; Inf, infinite.

lysis Buffer from the Magna RIP Kit (Millipore, Billerica, MA, USA). The beads were prepared according to protocol using rabbit dTDP-43 antibody (1:3,000), and normal rabbit IgG was used as a negative control. The pretreated beads and brain extracts were mixed and incubated ON at 4°C. Bound RNA transcripts were extracted according to protocol. First-strand synthesis was carried out according to the instructions of the Transcriptor first-strand cDNA synthesis kit (Roche). qRT-PCRs were performed with gene specific primers (see the Extended Experimental Procedures). In order to calculate the enrichment, the data were normalized to the inputs. The signal was represented by how many more fold increase was measured compared to the control signal. The error bars represent standard deviations on the normalized ratios. The statistical significance of differences observed was determined by t test ($p < 0.05$).

ACCESSION NUMBERS

The GEO database accession number for the RNA-seq data reported in this paper is GSE42844.

SUPPLEMENTAL INFORMATION

Supplemental Information includes Extended Experimental Procedures, five figures, and seven tables and can be found with this article online at http://dx.doi.org/10.1016/j.celrep.2012.12.014.

LICENSING INFORMATION

ACKNOWLEDGMENTS

L.V.B. and M.G. received PhD fellowships of the Agency for Innovation by Science and Technology in Flanders (IWT). M.N.S. and G.K. hold a PhD fellowship from the Foundation for Research Flanders (FWO) in Belgium. B.D. received a postdoctoral fellowship of the FWO and received support from the Foundation for Alzheimer Research (SAO/FRMA), FWO and the VIB Technology Watch Team in Belgium, and from Inserm, the University of Lille 2, DN2M (Démences des maladies Neurologiques et Mentales) as part of the contract project of the Etat Région Nord/Pas-de-Calais (grant 11005007) in France. P.C. is supported by VIB, FWO, and the Interuniversity Attraction Poles program P6/43 of the Belgian Science Policy Office (BELSPO). S.A. received support from the FWO (grant G.0704.11N) and KU Leuven (grants CREA/10/014 and PF/10/016) in Belgium and from the Human Frontier Science program (RGY0070/2011) and from the Foundation Against Cancer (grant 2010-154). F.H., Y.A., and D.C.D. were supported by grants from the Medical Research Council and the Royal Society, UK, and the Thierry Latran Foundation and

(B) Target and enhancer prediction analysis using the i-*cis*Target tool showing enrichment for the ERR recognition motif among the upregulated genes. Similarity between ERR and EcR is indicated. E-score, enrichment score.

(C) CCAP/bursicon-specific silencing (*ccap* > *dTDP-43^{RNAi}*) and overexpression (*ccap* > *dTDP-43*) of *dTDP-43* resulted in cytoplasmic accumulation (white arrows) of EcR-A (red) in the bursicon-positive neurons (green) in pharate adult ventral nerve cords. Scale bar, 10 μm.

See also Tables S6, S7, and Figure S4.

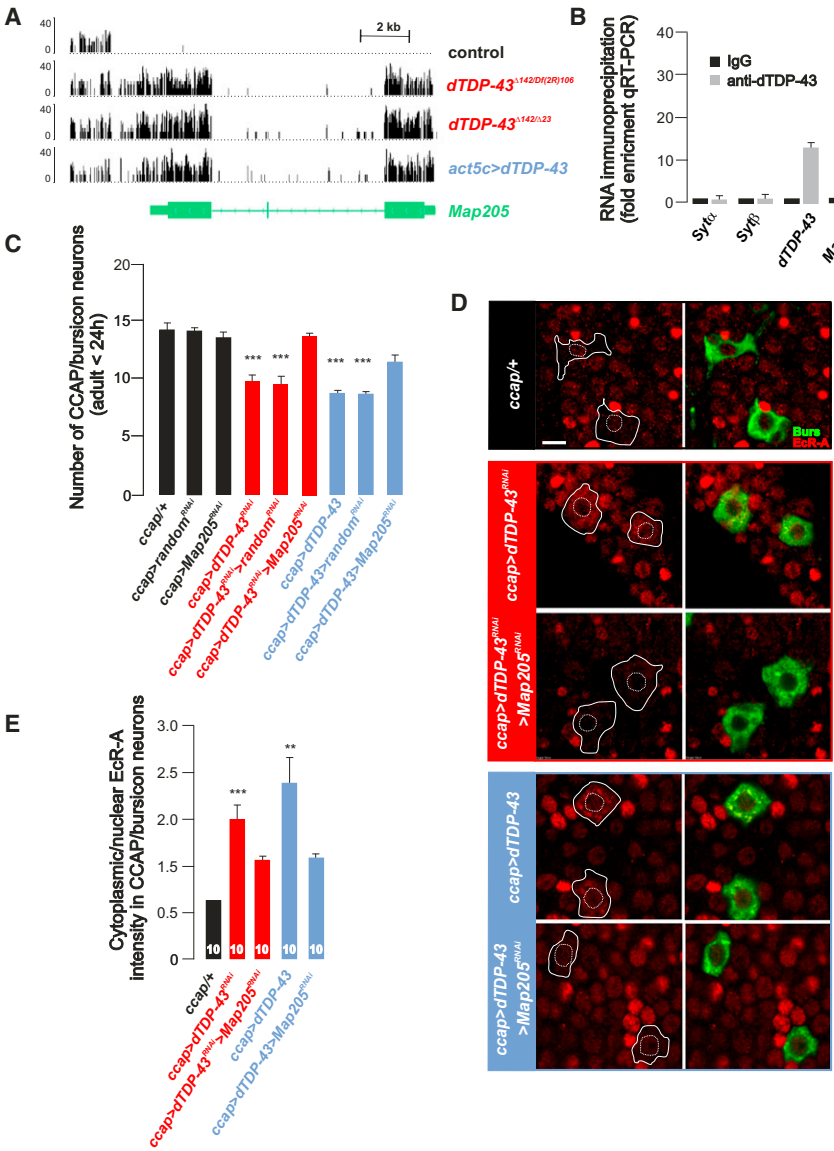

Figure 5. *dTDP-43*-Mediated Defective EcR Localization and Signaling Are Caused by Deregulated Expression of the Neuronal Microtubule-Associated Protein Map205

(A) RNA-seq reads showing the strong upregulation of *Map205* in *dTDP-43*$^{\Delta 23/\Delta 142}$, *dTDP-43*$^{\Delta 142/Df(2R)106}$, and *act5c* > *dTDP-43* late pupal heads.

(B) RNA immunoprecipitation analysis showing binding of dTDP-43 to *dTDP-43* and *Map205* mRNA but not to *Syt*α and *Syt*α mRNA.

(C) Loss of CCAP/bursicon neurons (adult flies < 8 hr after eclosion) by increased and decreased *dTDP-43* expression is suppressed by *Map205* knockdown. One-way ANOVA with post hoc Bonferroni test: ***$p \leq 0.001$, n = 10 for each genotype.

(D) Cytoplasmic accumulation of EcR-A induced by increased and decreased *dTDP-43* expression in CCAP/bursicon neurons is reduced by *Map205* knockdown. Bar = 5 μm.

(E) Increased ratio of cytoplasmic/nuclear EcR-A fluorescence intensity by increased and decreased *dTDP-43* expression is rescued by RNAi-mediated *Map205* silencing. **$p \leq 0.01$ ***$p \leq 0.001$. Error bars in (B), (C), and (E) represent SEM.

See also Figure S5.

the Motor Neurone Disease Association to F.H. C.V.B., and G.K received funding from the FWO, the Methusalem program of the Flemish Government, and the Interuniversity Attraction Poles program P6/43 of the Belgian Science Policy Office (BELSPO). We thank Christiane Hertz-Fowler at the Centre for Genomic Research (University of Liverpool, UK) for sequencing service and assistance in library preparation.

Received: February 13, 2012
Revised: October 29, 2012
Accepted: December 19, 2012
Published: January 17, 2013

REFERENCES

Aerts, S., Quan, X.J., Claeys, A., Naval Sanchez, M., Tate, P., Yan, J., and Hassan, B.A. (2010). Robust target gene discovery through transcriptome perturbations and genome-wide enhancer predictions in Drosophila uncovers a regulatory basis for sensory specification. PLoS Biol. *8*, e1000435.

Albrecht, M., and Lengauer, T. (2004). Survey on the PABC recognition motif PAM2. Biochem. Biophys. Res. Commun. *316*, 129–138.

Anders, S., and Huber, W. (2010). Differential expression analysis for sequence count data. Genome Biol. *11*, R106.

Andersson, S., Gustafsson, N., Warner, M., and Gustafsson, J.A. (2005). Inactivation of liver X receptor beta leads to adult-onset motor neuron degeneration in male mice. Proc. Natl. Acad. Sci. USA *102*, 3857–3862.

Arai, T., Hasegawa, M., Akiyama, H., Ikeda, K., Nonaka, T., Mori, H., Mann, D., Tsuchiya, K., Yoshida, M., Hashizume, Y., and Oda, T. (2006). TDP-43 is a component of ubiquitin-positive tau-negative inclusions in frontotemporal lobar degeneration and amyotrophic lateral sclerosis. Biochem. Biophys. Res. Commun. *351*, 602–611.

Bigini, P., Steffensen, K.R., Ferrario, A., Diomede, L., Ferrara, G., Barbera, S., Salzano, S., Fumagalli, E., Ghezzi, P., Mennini, T., and Gustafsson, J.A. (2010). Neuropathologic and biochemical changes during disease progression in liver X receptor beta-/- mice, a model of adult neuron disease. J. Neuropathol. Exp. Neurol. *69*, 593–605.

Budini, M., Baralle, F.E., and Buratti, E. (2011). Regulation of Gene Expression by TDP-43 and FUS/TLS in Frontotemporal Lobar Degeneration. Curr Alzheimer Res. *8*, 237–245.

Chiang, P.M., Ling, J., Jeong, Y.H., Price, D.L., Aja, S.M., and Wong, P.C. (2010). Deletion of TDP-43 down-regulates Tbc1d1, a gene linked to obesity, and alters body fat metabolism. Proc. Natl. Acad. Sci. USA *107*, 16320–16324.

Crossgrove, K., Bayer, C.A., Fristrom, J.W., and Guild, G.M. (1996). The Drosophila Broad-Complex early gene directly regulates late gene transcription during the ecdysone-induced puffing cascade. Dev. Biol. *180*, 745–758.

Feiguin, F., Godena, V.K., Romano, G., D'Ambrogio, A., Klima, R., and Baralle, F.E. (2009). Depletion of TDP-43 affects Drosophila motoneurons terminal synapsis and locomotive behavior. FEBS Lett. *583*, 1586–1592.

Freibaum, B.D., Chitta, R.K., High, A.A., and Taylor, J.P. (2010). Global analysis of TDP-43 interacting proteins reveals strong association with RNA splicing and translation machinery. J. Proteome Res. *9*, 1104–1120.

Graveley, B.R., Brooks, A.N., Carlson, J.W., Duff, M.O., Landolin, J.M., Yang, L., Artieri, C.G., van Baren, M.J., Boley, N., Booth, B.W., et al. (2011). The developmental transcriptome of Drosophila melanogaster. Nature *471*, 473–479.

Hanson, K.A., Kim, S.H., Wassarman, D.A., and Tibbetts, R.S. (2010). Ubiquilin modifies TDP-43 toxicity in a Drosophila model of amyotrophic lateral sclerosis (ALS). J. Biol. Chem. *285*, 11068–11072.

Hazelett, D.J., Chang, J.-C., Lakeland, D.L., and Morton, D.B. (2012). Comparison of parallel high-throughput RNA sequencing between knockout of TDP-43 and its overexpression reveals primarily nonreciprocal and nonoverlapping gene expression changes in the central nervous system of Drosophila. G3 (Bethesda) *2*, 789–802.

Herrmann, C., Van de, S.B., Potier, D., and Aerts, S. (2012). i-cisTarget: an integrative genomics method for the prediction of regulatory features and cis-regulatory modules. Nucleic Acids Res. *40*, e114.

Kabashi, E., Valdmanis, P.N., Dion, P., Spiegelman, D., McConkey, B.J., Vande Velde, C., Bouchard, J.P., Lacomblez, L., Pochigaeva, K., Salachas, F., et al. (2008). TARDBP mutations in individuals with sporadic and familial amyotrophic lateral sclerosis. Nat. Genet. *40*, 572–574.

Kabashi, E., Lin, L., Tradewell, M.L., Dion, P.A., Bercier, V., Bourgouin, P., Rochefort, D., Bel Hadj, S., Durham, H.D., Vande Velde, C., et al. (2010). Gain and loss of function of ALS-related mutations of TARDBP (TDP-43) cause motor deficits in vivo. Hum. Mol. Genet. *19*, 671–683.

Kim, H.J., Fan, X., Gabbi, C., Yakimchuk, K., Parini, P., Warner, M., and Gustafsson, J.A. (2008). Liver X receptor beta (LXRbeta): a link between beta-sitosterol and amyotrophic lateral sclerosis-Parkinson's dementia. Proc. Natl. Acad. Sci. USA *105*, 2094–2099.

King-Jones, K., and Thummel, C.S. (2005). Nuclear receptors—a perspective from Drosophila. Nat. Rev. Genet. *6*, 311–323.

Kraemer, B.C., Schuck, T., Wheeler, J.M., Robinson, L.C., Trojanowski, J.Q., Lee, V.M., and Schellenberg, G.D. (2010). Loss of murine TDP-43 disrupts motor function and plays an essential role in embryogenesis. Acta Neuropathol. *119*, 409–419.

Lagier-Tourenne, C., Polymenidou, M., and Cleveland, D.W. (2010). TDP-43 and FUS/TLS: emerging roles in RNA processing and neurodegeneration. Hum. Mol. Genet. *19*(R1), R46–R64.

Lee, E.B., Lee, V.M., and Trojanowski, J.Q. (2011). Gains or losses: molecular mechanisms of TDP43-mediated neurodegeneration. Nat. Rev. Neurosci. *13*, 38–50.

Li, Y., Ray, P., Rao, E.J., Shi, C., Guo, W., Chen, X., Woodruff, E.A., 3rd, Fushimi, K., and Wu, J.Y. (2010). A Drosophila model for TDP-43 proteinopathy. Proc. Natl. Acad. Sci. USA *107*, 3169–3174.

Lin, M.J., Cheng, C.W., and Shen, C.K. (2011). Neuronal function and dysfunction of Drosophila dTDP. PLoS ONE *6*, e20371.

Luan, H., Lemon, W.C., Peabody, N.C., Pohl, J.B., Zelensky, P.K., Wang, D., Nitabach, M.N., Holmes, T.C., and White, B.H. (2006). Functional dissection of a neuronal network required for cuticle tanning and wing expansion in Drosophila. J. Neurosci. *26*, 573–584.

Nedelsky, N.B., Pennuto, M., Smith, R.B., Palazzolo, I., Moore, J., Nie, Z., Neale, G., and Taylor, J.P. (2010). Native functions of the androgen receptor are essential to pathogenesis in a Drosophila model of spinobulbar muscular atrophy. Neuron *67*, 936–952.

Neumann, M., Sampathu, D.M., Kwong, L.K., Truax, A.C., Micsenyi, M.C., Chou, T.T., Bruce, J., Schuck, T., Grossman, M., Clark, C.M., et al. (2006). Ubiquitinated TDP-43 in frontotemporal lobar degeneration and amyotrophic lateral sclerosis. Science *314*, 130–133.

Park, J.H., Schroeder, A.J., Helfrich-Förster, C., Jackson, F.R., and Ewer, J. (2003). Targeted ablation of CCAP neuropeptide-containing neurons of Drosophila causes specific defects in execution and circadian timing of ecdysis behavior. Development *130*, 2645–2656.

Pereira, A., Doshen, J., Tanaka, E., and Goldstein, L.S. (1992). Genetic analysis of a Drosophila microtubule-associated protein. J. Cell Biol. *116*, 377–383.

Polymenidou, M., Lagier-Tourenne, C., Hutt, K.R., Huelga, S.C., Moran, J., Liang, T.Y., Ling, S.C., Sun, E., Wancewicz, E., Mazur, C., et al. (2011). Long pre-mRNA depletion and RNA missplicing contribute to neuronal vulnerability from loss of TDP-43. Nat. Neurosci. *14*, 459–468.

Ritson, G.P., Custer, S.K., Freibaum, B.D., Guinto, J.B., Geffel, D., Moore, J., Tang, W., Winton, M.J., Neumann, M., Trojanowski, J.Q., et al. (2010). TDP-43 mediates degeneration in a novel Drosophila model of disease caused by mutations in VCP/p97. J. Neurosci. *30*, 7729–7739.

Rolls, M.M., Satoh, D., Clyne, P.J., Henner, A.L., Uemura, T., and Doe, C.Q. (2007). Polarity and intracellular compartmentalization of Drosophila neurons. Neural Dev. *2*.

Saxena, S., and Caroni, P. (2011). Selective neuronal vulnerability in neurodegenerative diseases: from stressor thresholds to degeneration. Neuron *71*, 35–48.

Sendtner, M. (2011). TDP-43: multiple targets, multiple disease mechanisms? Nat. Neurosci. *14*, 403–405.

Sephton, C.F., Good, S.K., Atkin, S., Dewey, C.M., Mayer, P., 3rd, Herz, J., and Yu, G. (2010). TDP-43 is a developmentally regulated protein essential for early embryonic development. J. Biol. Chem. *285*, 6826–6834.

Sephton, C.F., Cenik, C., Kucukural, A., Dammer, E.B., Cenik, B., Han, Y., Dewey, C.M., Roth, F.P., Herz, J., Peng, J., et al. (2011). Identification of neuronal RNA targets of TDP-43-containing ribonucleoprotein complexes. J. Biol. Chem. *286*, 1204–1215.

Shan, X., Chiang, P.M., Price, D.L., and Wong, P.C. (2010). Altered distributions of Gemini of coiled bodies and mitochondria in motor neurons of TDP-43 transgenic mice. Proc. Natl. Acad. Sci. USA *107*, 16325–16330.

Sreedharan, J., Blair, I.P., Tripathi, V.B., Hu, X., Vance, C., Rogelj, B., Ackerley, S., Durnall, J.C., Williams, K.L., Buratti, E., et al. (2008). TDP-43 mutations in familial and sporadic amyotrophic lateral sclerosis. Science *319*, 1668–1672.

Tollervey, J.R., Curk, T., Rogelj, B., Briese, M., Cereda, M., Kayikci, M., König, J., Hortobágyi, T., Nishimura, A.L., Zupunski, V., et al. (2011). Characterizing the RNA targets and position-dependent splicing regulation by TDP-43. Nat. Neurosci. *14*, 452–458.

Trapnell, C., Roberts, A., Goff, L., Pertea, G., Kim, D., Kelley, D.R., Pimentel, H., Salzberg, S.L., Rinn, J.L., and Pachter, L. (2012). Differential gene and transcript expression analysis of RNA-seq experiments with TopHat and Cufflinks. Nat. Protoc. *7*, 562–578.

Truman, J.W., Talbot, W.S., Fahrbach, S.E., and Hogness, D.S. (1994). Ecdysone receptor expression in the CNS correlates with stage-specific responses to ecdysteroids during Drosophila and Manduca development. Development *120*, 219–234.

Vafopoulou, X. (2009). Ecdysteroid receptor (EcR) is associated with microtubules and with mitochondria in the cytoplasm of prothoracic gland cells of Rhodnius prolixus (Hemiptera). Arch. Insect Biochem. Physiol. *72*, 249–262.

Wang, J.W., Brent, J.R., Tomlinson, A., Shneider, N.A., and McCabe, B.D. (2011). The ALS-associated proteins FUS and TDP-43 function together to affect Drosophila locomotion and life span. J. Clin. Invest. *121*, 4118–4126.

Wang, L., Schuster, G.U., Hultenby, K., Zhang, Q., Andersson, S., and Gustafsson, J.A. (2002). Liver X receptors in the central nervous system: from lipid

homeostasis to neuronal degeneration. Proc. Natl. Acad. Sci. USA *99*, 13878–13883.

Wils, H., Kleinberger, G., Janssens, J., Pereson, S., Joris, G., Cuijt, I., Smits, V., Ceuterick-de Groote, C., Van Broeckhoven, C., and Kumar-Singh, S. (2010). TDP-43 transgenic mice develop spastic paralysis and neuronal inclusions characteristic of ALS and frontotemporal lobar degeneration. Proc. Natl. Acad. Sci. USA *107*, 3858–3863.

Wu, L.S., Cheng, W.C., Hou, S.C., Yan, Y.T., Jiang, S.T., and Shen, C.K. (2010). TDP-43, a neuro-pathosignature factor, is essential for early mouse embryogenesis. Genesis *48*, 56–62.

Wu, L.-S., Cheng, W.-C., and Shen, C.-K. (2012). Targeted depletion of TDP-43 expression in the spinal cord motor neurons leads to the development of amyotrophic lateral sclerosis (ALS)-like phenotypes in mice. J. Biol. Chem. Published online June 20, 2012. http://dx.doi.org/10.1074/jbc.M112.359000.

Xu, Z.S. (2012). Does a loss of TDP-43 function cause neurodegeneration? Mol. Neurodegener. *7*, 27.

Ye, Y., and Fortini, M.E. (1999). Apoptotic activities of wild-type and Alzheimer's disease-related mutant presenilins in Drosophila melanogaster. J. Cell Biol. *146*, 1351–1364.

Zhao, T., Gu, T., Rice, H.C., McAdams, K.L., Roark, K.M., Lawson, K., Gauthier, S.A., Reagan, K.L., and Hewes, R.S. (2008). A Drosophila gain-of-function screen for candidate genes involved in steroid-dependent neuroendocrine cell remodeling. Genetics *178*, 883–901.

Zhou, X., and Riddiford, L.M. (2002). Broad specifies pupal development and mediates the 'status quo' action of juvenile hormone on the pupal-adult transformation in Drosophila and Manduca. Development *129*, 2259–2269.